[Research Paper] 대한금속 · 재료학회지 (*Korean J. Met. Mater.*), Vol. 62, No. 2 (2024) pp.106-114
DOI: 10.3365/KJMM.2024.62.2.106

Modulating the Electrical Properties of Lithium-Doped Zinc Oxide: Interplay of Lithium Content, Oxygen Pressure, and Temperature

Byoungnam Park*

Department of Materials Science and Engineering Hongik University 72-1, Sangsu-dong, Mapo-gu, Seoul 04066, Republic of Korea

Abstract: This research elucidates the intricate interplay of lithium content, oxygen pressure, and temperature and their influence on the electrical properties of Lithium-doped zinc oxide (LZO). The electrical behavior of zinc oxide (ZnO), a prominent semiconductor material, can be modulated when doped with lithium (Li). Through systematic experimentation, we demonstrate that varying lithium content in the ZnO matrix leads to notable shifts in carrier concentration and mobility, which in turn impacts the material's conductivity and overall electrical performance. Furthermore, oxygen pressure during synthesis plays a pivotal role in defect formation, especially oxygen vacancies, which interact dynamically with lithium dopants to further modulate electrical behavior. Introducing the variable of temperature, our study reveals a synergistic effect, where temperature not only affects intrinsic carrier concentration but also the interactions between lithium dopants and inherent defects in ZnO. Under optimized conditions of oxygen pressure and temperature, the influence of Li content on crystallinity was pronounced, consequently impacting mobility. In contrast, under unoptimized conditions, as Li concentration increased, particularly beyond optimal levels (0.75 mol%), introduced Li atoms assumed the role of compensating centers by capturing or neutralizing carriers, reducing mobility. The findings presented herein provide a comprehensive understanding of how these factors collectively determine the electrical properties of LZO, paving the way for tailored applications in optoelectronic devices, sensors, and more.

(Received 6 October, 2023; Accepted 9 November, 2023)

Keywords: zinc oxide, Li-doping, mobility, field effect transistor, carrier concentration

1. Introduction

Zinc Oxide (ZnO) stands out among the myriad semiconductor materials because of its rich set of optical, electrical, and piezoelectric properties [1-5]. Its wide bandgap of approximately 3.37 eV at room temperature and its large exciton binding energy make it an attractive choice for optoelectronic devices, solar cells, and sensors [6-9]. However, despite its numerous advantages, the intrinsic electrical properties of ZnO often necessitate modification to render it suitable for specific applications.

To optimize ZnO's electronic characteristics, researchers have employed various doping methods, introducing foreign atoms into the ZnO lattice. Doping not only modulates electrical conductivity but also affects other physical properties, thereby allowing customization of the material's performance [10, 11]. Among the various dopants studied to enhance ZnO's electrical properties, Li has emerged as a promising candidate. Li, being the lightest metal and having a smaller ionic size compared to zinc, offers unique interactions when introduced into the ZnO lattice [12-15]. Recent studies have begun to elucidate intriguing potential benefits of Li doping and the mechanisms behind them. Park et. al reported a boost in the performance of solution-processed ZnO thin-film transistors (TFTs) by using Li and sodium (Na) as dopants [16]. A unique low-temperature fabrication method was developed, allowing the creation of carbon-free ZnO thin films as TFT active layers at just 300°C. Results showed that both Li-doped and Na-doped ZnO TFTs achieved impressive field-effect mobilities, with Li-doped devices reaching up to 11.45 $cm^2\ V^{-1}\ s^{-1}$. They also exhibited excellent on/off ratios exceeding 10^7. Importantly, all these devices were processed

- 박병남: 교수
Corresponding Author: Byoungnam Park
[Tel: +82-2-320-1631, E-mail: metalpbn@hongik.ac.kr]
Copyright ⓒ The Korean Institute of Metals and Materials

at low temperatures, making them suitable for flexible electronics, particularly on plastic substrates.

Bang et. al reported LZO films created through a simple solution process, which exhibited improved crystallinity and smoother surfaces compared to undoped ZnO films. LZO TFTs on heavily p-doped Si substrates achieved a peak field-effect mobility of 5.18 $cm^2 V^{-1} s^{-1}$ with an on/off ratio of 10^7, demonstrating the effectiveness of Li doping for enhancing ZnO film properties and TFT performance [17]. Aksoy et. al employed microwave-assisted hydrothermal synthesis to create LZO nanopowders [18]. Their structural properties, morphological characteristics, and photovoltaic performance in dye-sensitized solar cells (DSSCs) were investigated [14]. Notably, the DSSCs using these nanopowders achieved an efficiency of 1.23%, surpassing previous studies and demonstrating the potential of LZO for enhancing DSSC performance [18]. Hjiri et. al. studied Li-doping-induced structural and optical properties associated with defects [14]. LZO films were produced using sol-gel spin coating, with Li doping levels ranging from 0% to 10%. XRD analysis confirmed a hexagonal Wurtzite structure in both doped and undoped films. Li doping induced a red shift in the absorption edge in UV-Vis spectroscopy. PL spectra didn't reveal distinct Li-related peaks, suggesting that Li defects were obscured within the band tail width states. This suggests that Li doping promotes oxygen vacancy defects in ZnO films rather than oxygen interstitial defects. Rajeevgandhi et. al demonstrated that spherical LZO nanoparticles via co-precipitation exhibited supercapacitor behavior with a specific capacitance of 401 F/g at a scan rate of 2 mV/s [19]. Metal oxide semiconducting (MOS) gas sensors using ZnO films were characterized and evaluated for NO_2 gas sensing [20]. Undoped and alkali-metal (Li/Na)-doped ZnO films were compared. The LZO sensors exhibited higher sensitivity and faster response/recovery times, detecting NO_2 at 15 ppm, below the exposure limit (20 ppm).

The current literature presents varying results concerning the electrical, structural, and optical effects of lithium doping on ZnO [6, 21, 22]. Some suggest an enhancement in conductivity and carrier concentration, while others have revealed potential challenges [12, 23, 24]. This disparity in outcomes underscores the necessity for a systematic and comprehensive study of LZO, as groundwork for this research endeavor.

Optimizing the electrical properties of ZnO through Li doping could have a significant impact on various industries. Enhanced electrical properties could lead to more efficient electronic devices, better solar cells, or more sensitive sensors. Furthermore, as the global electronics industry moves towards more sustainable and efficient materials, understanding and leveraging the potential of LZO will become paramount.

The primary goal of this research is to present a comprehensive understanding of how lithium doping affects ZnO's electrical properties. In particular, we focused on the LZO thin film close to the gate dielectric, by adopting a bottom-contact field effect transistor (FET) configuration. Through systematic experiments we aim to quantify the improvements (or detriments) in electrical properties and to understand the underlying mechanisms driving these changes. We propose optimal doping concentrations and methods to achieve the desired electrical characteristics.

2. Materials and Methods

2.1 Preparation of the Zn Precursor Solution:

Zinc acetate dihydrate was dissolved in 2-methoxyethanol to achieve a concentration of 0.8M. The solution was prepared using 5mL of 2-methoxyethanol as the solvent. Subsequently, ethanolamine, serving as a stabilizer, was introduced to the solution in quantities equimolar with the Zn ions. The resulting mixture was then stirred at 75°C for a duration of 2 hours. The completely dissolved solution underwent filtration using a polytetrafluoroethylene (PTFE) syringe filter with a pore size of 0.2μm. Following filtration, the solution was allowed to age in ambient air for a period of 48 hours.

2.2 Lithium Doping Process

Lithium acetate dihydrate was added to the Zn precursor solution to achieve Li doping concentrations of 0.25, 0.50, and 0.75 mol%. After thorough mixing, the solution was stirred at room temperature for 2 hours. The homogenized mixture was then subjected to filtration through a 0.2μm pore PTFE syringe filter. All of the containers utilized during this procedure had been meticulously cleaned with acetone, methanol, and deionized (DI) water.

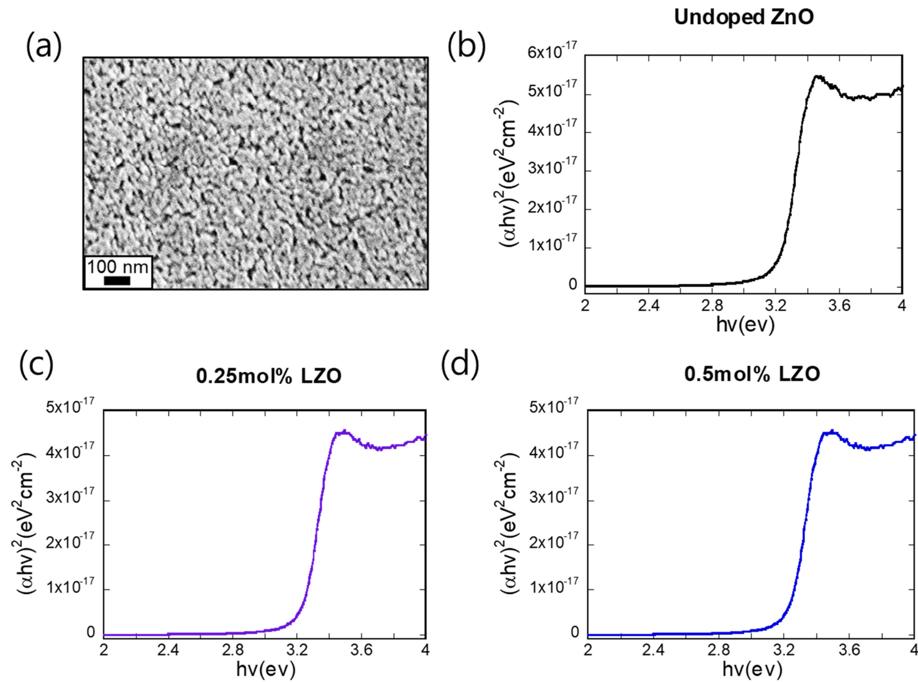

Fig. 1. (a) An SEM image of undoped ZnO at a thickness of 60 nm Tauc plots of (b) undoped (c) 0.25mol% Li-doped and (d) 0.5mol% LZO.

2.3 Substrate Preparation

A highly doped silicon (Si) substrate, featuring a 200nm thick SiO_2 layer, was cleaned using a sequential sonication process in acetone, methanol, and DI water, each for 10 minutes. This was followed by a UV-ozone treatment for 5 minutes. Subsequently, the cleaned substrate was spin-coated with the prepared solution at 3000 rpm for 30 seconds. Patterning of the coated film was carried out, followed by a soft annealing process on a hot plate set to 250°C for 5 minutes, facilitating the evaporation of any residual solvents.

2.4 Oxidation Process

The precursor-coated film underwent an oxidation process for 1 hour via the rapid thermal annealing (RTA) method. Both the oxidation temperature and the oxygen partial pressure were maintained at constant values during the RTA process. The final thickness of the oxidized film was approximately 60 nm.

2.5 Device Fabrication, and Electrical/Structural Characterizations

For the final device assembly, aluminum (Al) electrodes with a thickness of 100 nm were thermally evaporated onto the oxidized film. This facilitated the fabrication of a field-effect transistor (FET) with defined channel dimensions: a length of 60 μm and a width of 6 mm. FET characteristic curves were measured using HP4145B in an Ar-filled glovebox. The surface morphology and structural characteristics of the ZnO films were investigated by scanning electron microscopy (SEM) and X-ray diffraction (XRD) using CuKa radiation (λ=1.54178 Å). Photoluminescence (PL) measurements were conducted at room temperature, utilizing the He–Cd laser line at 325 nm.

3. Results and Discussion

Figure 1(a) presents an SEM image of a ZnO film deposited via spin-coating on a SiO_2 substrate. Notably, void spaces are discernible between individual ZnO grains following the drying process. To explore charge transport in proximity to the gate dielectric under carrier accumulation conditions, we intentionally limited the film thickness to approximately 60 nm in the bottom-contact FET configuration. Figures 1(b), 1(c), and 1(d) depict the optical absorption data for the ZnO and LZO films. With increasing

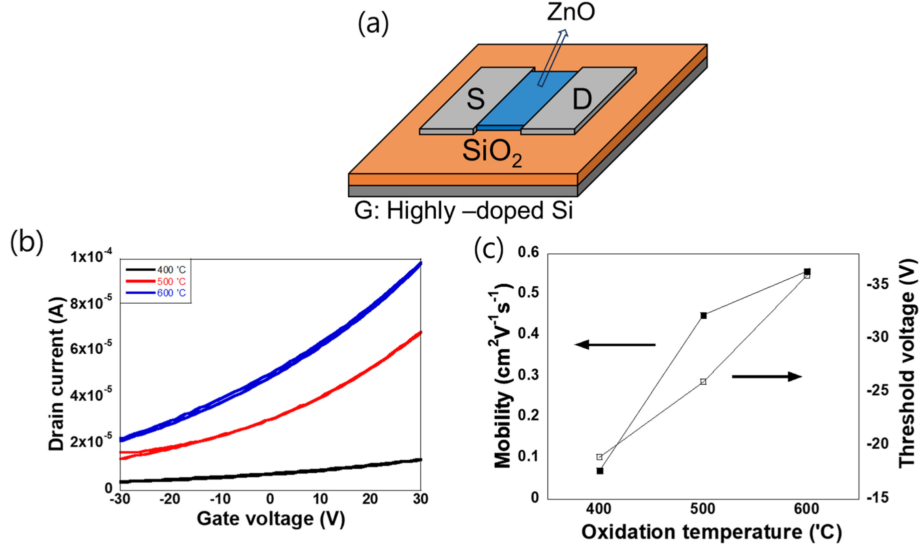

Fig. 2. (a) A schematic of ZnO FET structure. (b) I_D-V_G plots at a constant drain voltage of 5 V for different oxidation temperatures of 400, 500, and 600°C (P_{O2}=0.4 torr). (c) Plots of mobility and threshold voltage as a function of oxidation temperature.

Li content, a slight increase in the band gap was observed, shifting from 3.217 eV (in non-doped ZnO) to 3.232 eV (in 0.5mol% LZO). This rise can be attributed to the Burstein-Moss effect, which results from the occupation of lower energy states in the conduction band by surplus carriers, causing an apparent shift in the absorption edge toward higher energies [25, 26]. The electrical properties of ZnO were measured using FET devices in which source and drain Al (100nm) electrodes were deposited on the ZnO layer. In the FET structure, the drain current (I_D) arises due to the movement of charge carriers, either electrons (in *n*-type FETs) or holes (in *p*-type FETs), between the source and drain electrodes, modulated by the gate voltage (V_G). The behavior of the drain current is typically characterized by two regimes: the linear regime and the saturation regime. Here we measured the FET mobility and the threshold voltage (V_T) in the linear regime. The magnitude of the drain current (I_D) is determined by the mobility (μ) and carrier concentration ($n=C_i(V_G-V_T)/q$), as given in the equation,

$$I_D = \frac{Z}{L}\mu C_i(V_G - V_T)V_D$$

, where L, Z, *and* C_i represent the channel width, length, and the capacity of the gate dielectric respectively. The threshold voltage (V_T) is the gate voltage (V_G) used to induce mobile carriers in the channel, a measure of electron carrier concentration.

We systematically examined the impact of oxidation temperature, under constant oxygen pressure, on the Field-Effect Transistor (FET) mobility and the threshold voltage of the undoped ZnO, as illustrated in Figure 2.

The FET structure (depicted in Figure 2(a)) showed *n*-channel FET behavior, with the drain current increasing alongside rising gate voltage (V_G), as depicted in the V_G-I_D curve in Figure 2(b).

Notably, with increasing oxidation temperature, the I_D-V_G curve displayed an augmented slope within the linear region, indicating an enhancement in FET mobility. These variations in FET mobility and threshold voltage in relation to oxidation temperature are illustrated in Figure 2(c). As oxidation temperature increased, FET mobility exhibited a corresponding rise in threshold voltage (indicating electron concentration) decreasing (increasing electron carrier concentration) from -19 V (400°C) to -36 V (600°C). This increase in FET mobility and electron concentration is attributed to improved crystalline quality, grain growth, and a reduction in defect density, factors that will be discussed in detail later.

Li doping introduces an additional layer of complexity into the system. Figure 3 illustrates the variations in mobility according to Li content in ZnO under different oxygen pressures and oxidation temperatures.

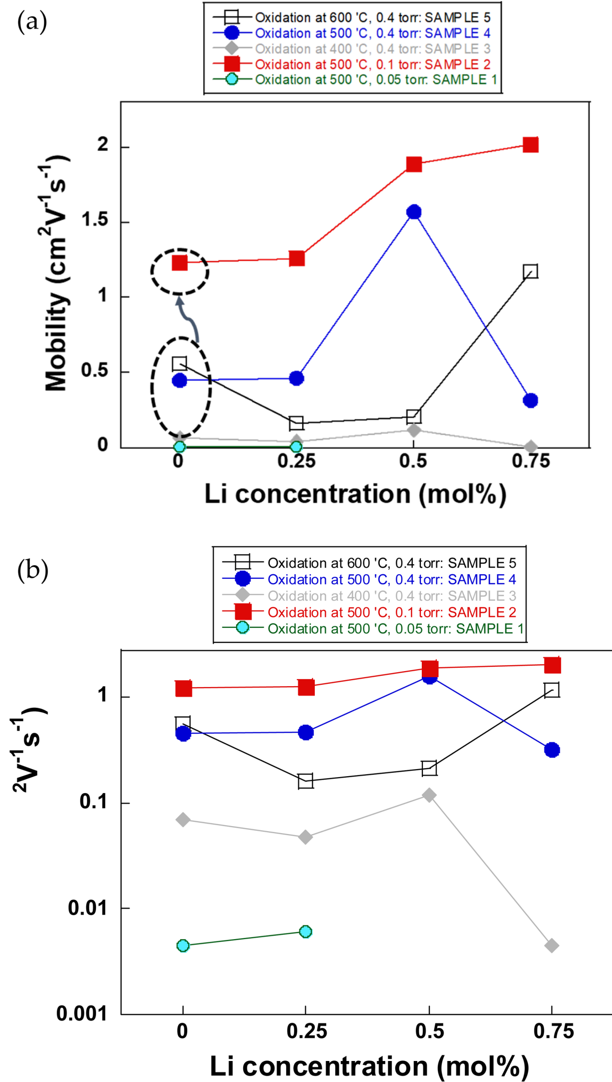

Fig. 3. (a) Plots of mobility as a function of Li concentration for five samples on a linear scale. (b) Plots of mobility as a function of Li concentration for five samples on a semi-logarithmic scale.

Notably, in non-doped ZnO, reducing oxygen pressure from 0.4 torr to 0.1 torr resulted in a remarkable increase in mobility as marked in Figure 3(a). For sample 3, the FET mobility increased from 0.07 to 1.23 cm^2/Vs. This phenomenon is attributed to the formation of oxygen vacancies (Vo) in ZnO, acting as donor defects that contribute free electrons to the conduction band, thereby enabling n-type conductivity [27, 28].

Reducing oxygen pressure during growth enhances oxygen vacancy formation, subsequently raising the electron carrier concentration. While increased electron concentration may appear advantageous for conductivity, it can also introduce elevated electron-electron scattering, which often leads to reduced mobility. However, if the rise in free electrons is within a certain range or if alternative scattering mechanisms (e.g., phonon scattering or defect scattering) are mitigated at lower oxygen pressures, an overall mobility enhancement is observed. Another potential factor contributing to increased mobility is the improved crystalline quality of the ZnO film due to reduced oxygen pressure. Enhanced crystallinity translates to fewer grain boundaries and defects, minimizing scattering events and thus promoting higher mobility. Notably, our XRD results did not detect significant changes in (002) peak intensity in relation to these effects.

The dramatic increase in mobility at reduced oxygen pressure suggests that, in this pressure range, the benefits (increased free carriers and possibly improved crystallinity) outweigh the potential downsides (increased electron-electron scattering) associated with a reduced oxygen environment. At a very low oxygen pressure of 0.05 torr, the mobility of the LZO was very low, at 500℃, with the Li content between 0 and 0.75 mol%, as clearly seen in Figure 3(b) (semi-logarithmic plot of Figure 3(a)), independent of Li content. At very low oxygen pressures, the formation of oxygen vacancies becomes predominant. These vacancies act as shallow donors in ZnO and can trap electrons, thus increasing scattering events and reducing electron mobility. While the concentration of electrons (carrier concentration) is increased by oxygen vacancies, this does not guarantee increased mobility. Oxygen vacancies can act as scattering centers for conduction electrons, leading to a higher frequency of electron scattering events, reducing overall mobility [29, 30].

At low Li doping concentrations, specifically up to 0.5 mol%, the trend in mobility variations was similar for doped and non-doped ZnO. However, a noteworthy transition occurred when Li was introduced in higher concentrations, particularly from 0.5 mol% to 0.75 mol%. During this transition, a significant drop in the FET mobility was observed in samples 3 and 4.

When Li substitutes for zinc (Li_{Zn}), it assumes the role of an acceptor in the ZnO lattice. Consequently, Li_{Zn} can effectively capture some of the free electrons, thus mitigating the overall increase in electron concentration stemming from oxygen vacancies (V_O) [31, 32]. This introduces a competitive

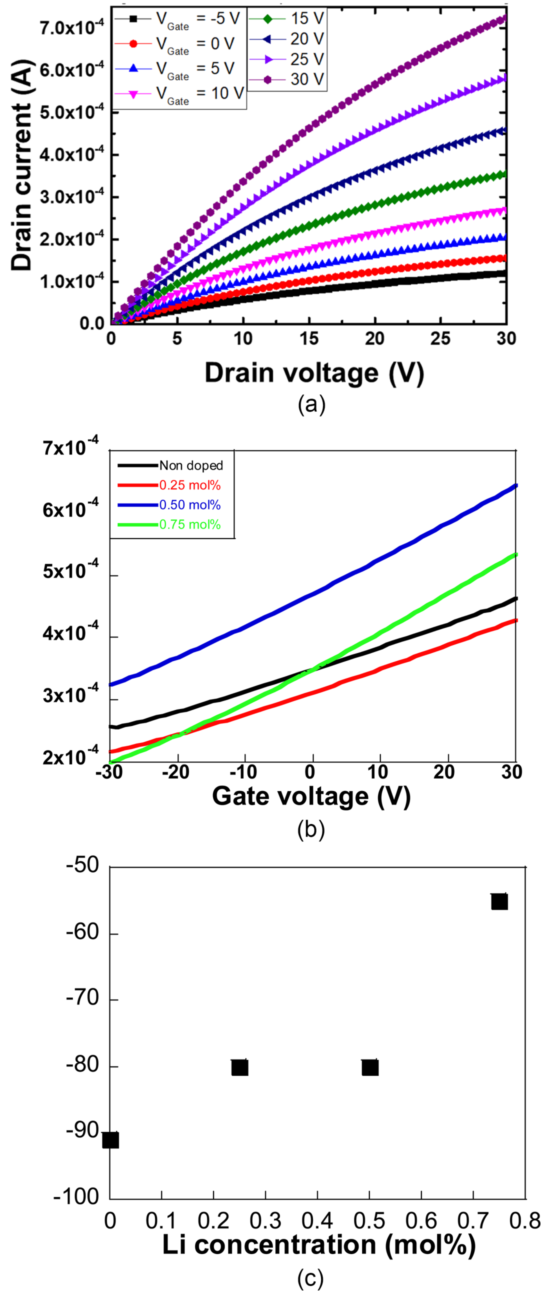

Fig. 4. (a) Transistor I_D-V_D output characteristic curves for 0.5mol% Li-doping of sample 2. (b) Plots of I_D-V_G transfer characteristic curves varying Li concentration for sample 2. (b) A plot of threshold voltage as a function of Li-concentration.

dynamic: while V_O introduces electrons, Li_{Zn} has the capacity to capture some of these electrons. Furthermore, it's worth noting that Li can also act as a shallow donor, similar in function to V_O.

Figures 4(a) and 4(b) show the transistor output (0.5 mol% LZO) and transfer characteristic curves for sample 2, respectively. In the optimized condition (sample 2), mobility significantly outperformed other samples (samples 1, 3, 4, and 5) and exhibited a consistent increase with rising Li concentration. A noteworthy observation was the shift in the threshold voltage to a more positive value (increase), indicating a concurrent reduction in electron carrier concentration, as depicted in Figure 4(c). In essence, mobility was enhanced at the same time the electron carrier concentration decreased, signifying an improvement in the electronic properties of ZnO.

This improvement could be attributed to several factors, including the reduction in the number of scattering centers within the lattice, and enhancements in crystallinity or grain boundary structure [30, 33]. Significantly, Figure 5(a) illustrates the emergence of the (002) peak as Li content increased from 0.25 to 0.5 mol% Li doping, indicating a pronounced preference for c-axis orientation. Consequently, the persistent increase in FET mobility with Li content, even in the face of declining carrier concentration, can be attributed to heightened crystallinity. Therefore, in the optimized condition of sample 2, mobility changes appeared to be sensitive to crystallinity. This is supported by the fact that the mobility remained the same while Li concentration increased from 0 to 0.25 mol%, and no improvements in crystallinity were observed when Li content increased from 0 to 0.25 mol%, as shown in Figure 5.

It's crucial to highlight that the concentration of oxygen vacancy defects remained consistent across different Li concentrations, as evidenced by the PL measurements in Figure 5(b), which show there were no significant changes in the intensity of the green emission at 520 nm as Li concentration increased. This green emission is typically associated with oxygen vacancy defects [30, 34]. Hence, it's clear that alterations in mobility related to varying Li content were unrelated to oxygen vacancy defects. Additionally, we did not observe substantial changes in surface morphology with different Li content.

In contrast to the optimized condition (sample 2), where mobility consistently increased with Li concentration, samples 3 and 4 exhibited a trend of mobility peaking at a certain Li concentration and then subsequently declining, despite a continuous rise in carrier concentration. This behavior underscores the intricate interplay of doping

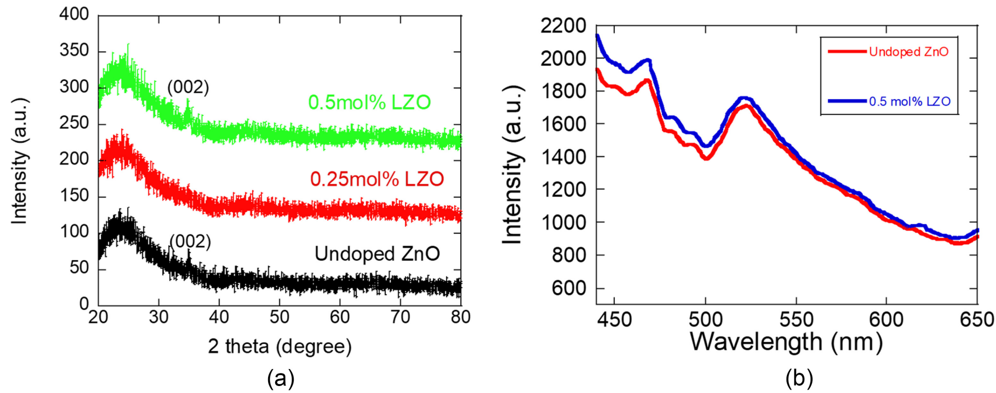

Fig. 5. (a) XRD data for undoped ZnO, 0.25mol% LZO, and 0.5mol% LZO. (b) Plots of PL intensity as a function of wavelength for undoped ZnO and 0.5mol% LZO.

mechanisms, defect interactions, and microstructural alterations within the ZnO matrix.

More specifically, the incorporation of Li into the ZnO matrix involves distinct site preferences: Li, when replacing zinc (Li_{Zn}), acts as an acceptor, resulting in carrier depletion.[35] Conversely, Li residing in interstitial sites (Li_i) acts as a donor, facilitating carrier contribution.[36] [21] At lower doping levels, these effects might balance, resulting in higher mobility. However, at higher doping levels, other factors, such as the clustering of Li or the formation of complex defects, may dominate.[37] As Li concentration increases, especially beyond optimal levels, some introduced Li atoms might serve as compensating centers. In this capacity, they introduce carriers while simultaneously capturing or neutralizing other carriers, thus increasing carrier concentration without a corresponding increase in mobility. Additionally, overdoping or clustering of Li can create deep-level traps, which can impede carrier movement and lower mobility.

An upward trend in the FET mobility for undoped ZnO in Figure 2 was observed with increasing oxidation temperature, suggesting enhanced electronic transport properties. At higher temperatures, the equilibrium concentration of oxygen vacancies (Vo) in ZnO increases [28]. This is because higher temperatures provide more thermal energy to promote the formation of vacancies in the crystal lattice. As the concentration of oxygen vacancies rises, it can introduce more free electrons into the crystal, thereby increasing the carrier concentration, consistent with the negative shift of the threshold voltage in an *n*-channel FET. These vacancies can introduce additional free electrons into the crystal, increasing carrier concentration. As electrons from these vacancies fill other trap sites, the life-times of electrons increase, resulting in enhanced mobility. An increase in carrier concentration, if not offset by other factors like increased scattering mechanisms, leads to higher electrical mobility. The increase in electrical mobility in undoped ZnO with higher oxidation temperature can be explained, at least in part, by the higher equilibrium concentration of oxygen vacancies at elevated temperatures.

4. Conclusion

In this study, we systematically investigated the influence of oxidation temperature, oxygen pressure, and lithium doping on FET mobility and the threshold voltage of ZnO films. Most of all we directly investigated the ZnO film close to the gate dielectric, using a thin ZnO film. A notable elevation in mobility was identified when the oxygen pressure was reduced from 0.4 torr to 0.1 torr for undoped ZnO. Oxygen vacancies, serving as donor defects in ZnO, are amplified under diminished oxygen pressure, enhancing the electron carrier concentration. However, increased carrier concentration can also augment electron-electron scattering, potentially impeding mobility. The sharp increase in mobility suggests that the advantages of elevated free carriers, potentially coupled with heightened crystallinity, overcomes the limitations imposed by increased scattering at these oxygen pressures. Intriguingly, at an extremely low oxygen pressure of 0.05 torr, mobility dwindled considerably,

possibly due to excessive oxygen vacancies acting as electron traps and scattering sites.

LZO exhibited intriguing behavior. Up to 0.5 mol% of Li doping, the mobility patterns mirrored those of undoped ZnO. Yet, a stark decline in mobility was observed as the doping was increased to 0.75 mol%. Lithium, when substituting zinc, behaves as an acceptor in ZnO, capturing some free electrons and thus potentially opposing the electron-boosting effect of oxygen vacancies. This intricate interplay governs the observed mobility trends.

In optimized conditions at 0.5 mol% Li doping, an increase in Li content was concomitant with an upswing in mobility. Concurrently, a positive shift in the threshold voltage indicated a reduction in electron carrier concentration. These observations hint at a synergistic effect, where Li doping helps to minimize certain scattering centers and perhaps refine crystalline properties. Indeed, XRD data corroborated this by revealing a preferential c-axis orientation at this doping level.

In conclusion, the results underscore the delicate balance and interplay between defect engineering, crystalline quality, and external parameters like oxidation temperature and oxygen pressure in modulating the electronic properties of ZnO. Li doping offers a potent tool to fine-tune these properties, with implications for enhancing the performance of ZnO-based electronic devices. The precise tuning of Li-doping levels, combined with controlled annealing processes, is crucial to optimize both carrier concentration and mobility in LZO. Further investigations using techniques like transmission electron microscopy (TEM) for structural analysis or deep level transient spectroscopy for defect state characterization might provide more insights into the observed trends.

ACKNOWLEDGEMENT

This research was supported by the Basic Science Research Program through the National Research Foundation of Korea (NRF) funded by the Ministry of Education (NRF-2015R1A6A1A03031833, and NRF-2020R1A2C1007258). This work was also supported by the 2024 Hongik Faculty Research Support Fund.

REFERENCES

1. Teklemichael S., McCluskey M., *Nanotechnology* **22**, 475703 (2011).
2. Look D. C., *Materials science and engineering: B* **80**, 383 (2001).
3. Kim M., Han C.-Y., Yang H., Park B., *Materials* **12**, 2289 (2019).
4. Kim Y., Park B., *Results in Physics* **13**, 102207 (2019).
5. Chang M., Park B., *Materials Letters* **306**, 130909 (2022).
6. Özgür Ü., Alivov Y. I., Liu C., Teke A., Reshchikov M., Doğan S., Avrutin V., Cho S.-J., Morkoç, *Journal of Applied Physics* **98**, 11 (2005).
7. Ü. Özgür, D. Hofstetter and H. Morkoç, *Proceedings of the IEEE* **98**, 1255 (2010).
8. Wibowo, A. Marsudi, M. A. Amal, M. I. Ananda, M. B. Stephanie, R. Ardy, H. Diguna, L. J., *RSC advances* **10**, 42838 (2020).
9. Franco, M. A., Conti, P. P., Andre, R. S., Correa, D. S., *Sensors and Actuators Reports* **4**, 100100 (2022).
10. Norton, D. P., Heo, Y., Ivill, M., Ip, K., Pearton, S., Chisholm, M. F., Steiner, T., *Materials Today* **7**, 34 (2004).
11. Xiu, F., Xu, J., Joshi, P. C., Bridges, C. A., Parans Paranthaman, M., *Semiconductor Materials for Solar Photovoltaic Cells* **218**, 105 (2016).
12. Zeng, Y., Ye, Z., Xu, W., Li, D., Lu, J., Zhu, L., Zhao, B., *Applied Physics Letters* **88**, 062107 (2006).
13. Jeong, S., Park, B., Lee, S.-B., Boo, J.-H., *Thin Solid Films* **516**, 5586 (2008).
14. Hjiri, M., Aida, M., Lemine, O., El Mir, L., Materials *Science in Semiconductor Processing* **89**, 149 (2019).
15. Alexandrov, A., Zvaigzne, M., Lypenko, D., Nabiev, I., Samokhvalov, P., *Scientific Reports* **10**, 7496 (2020).
16. Park, S. Y., Kim, B. J., Kim, K., Kang, M. S., Lim, K. H., Lee, T. I., Myoung, J. M., Baik, H. K., Cho, J. H., Kim, Y. S., *Advanced Materials* **24**, 834 (2012).
17. Bang, K., Son, G.-C., Son, M., Jun, J.-H., An, H., Baik, K. H., Myoung, J.-M., Ham, M.-H., *Journal of Alloys and Compounds* **739**, 41 (2018).
18. Aksoy, S., Polat, O., Gorgun, K., Caglar, Y., Caglar, M., Physica E: Low-dimensional Systems and Nanostructures 121, 114127 (2020).19. Rajeevgandhi, C., et al., *Solid State Communications* **371**, 115256 (2023).
19. Rajeevgandhi, C., Bharanidharan, S., Jayakumar, T., Shailaja, N., Anand, P., Guganathan, L., Balasubhramanyam, P, *Solid State Communications* **371**, 115256 (2023).

20. Jasmi, K. K., et al., AIP Conference Proceedings, 030006, AIP Publishing, India (2023).
21. Lu, J. G., et al., *Applied Physics Letters* **89**, 11 (2006).
22. Wang, Jie, et al., *ACS Applied Materials & Interfaces* **14**, 12450 (2022).
23. Wardle, M. G., J. P. Goss, and P. R. Briddon., *Physical Review B* **71**, 155205 (2005).
24. Kim, Jeongeun, et al., *Energy Technology* **11**, 2201453 (2023).
25. Mayekar, Jyoti., IJRAR **9**, 1 (2022).
26. Campbell, Bethany, et al., *Metamaterials, Metadevices, and Metasystems 2020* **11460**, 11460H (2020).
27. Lei, Jing, et al., *Analytical Chemistry* **94**, 8642 (2022).
28. Xiong, Xin, et al., *Applied Surface Science* **616**, 156556 (2023).
29. Pramanik, Subhamay, et al., *Journal of Alloys and Compounds* **849**, 156684 (2020).
30. Gurylev, Vitaly, and Tsong Pyng Perng, *Journal of the European Ceramic Society* **41**, 4977 (2021).
31. Galdámez-Martinez, Andres, et al., *Nanomaterials* **10**, 857 (2020).
32. Chithira, P. R., and Teny Theresa John, *Journal of Luminescence* **185**, 212 (2017).
33. Nadupalli, Shankari, et al., *Nanoscale* **13**, 9160 (2021).
34. Leung, Y. H., et al., *Applied Surface Science* **271** 202 (2013).
35. Rauch, Christian, et al., *Journal of Applied Physics*, **107**, 2 (2010).
36. Zhang, Z., et al., *Applied Physics* **45**, 375301 (2012).
37. Zhang, Z., et al., *Applied Physics Letters* **100**, 4 (2012).